LAWRENCE
LIVERMORE
NATIONAL
LABORATORY

LLNL-PROC-492911

RAYLEIGH-TAYLOR STRENGTH EXPERIMENTS OF THE PRESSURE-INDUCED alpha->epsilon->alpha' PHASE TRANSITION IN IRON

J. L. Belof, R. M. Cavallo, R. T. Olson, R. S. King, G. T. Gray, D. B. Holtkamp, S. R. Chen, R. E. Rudd, N. R. Barton, A. Arsenlis, B. A. Remington, H. Park, S. T. Prisbrey, P. A. Vitello, G. Bazan, K. O. Mikaelian, A. J. Comley, B. R. Maddox, M. J. May

August 11, 2011

Rayleigh-Taylor Strength Experiments of the Pressure-Induced alpha->epsilon->alphaprime Phase Transition in Iron
Chicago, IL, United States
June 26, 2011 through July 2, 2011

Disclaimer

RAYLEIGH-TAYLOR STRENGTH EXPERIMENTS OF THE PRESSURE-INDUCED $\alpha \rightarrow \varepsilon \rightarrow \alpha'$ PHASE TRANSITION IN IRON

Jonathan L. Belof[*], Robert M. Cavallo[*], Russell T. Olson[†], Robert S. King[†], George T. Gray III[†], David B. Holtkamp[†], Shuh-Rong Chen[†], Robert E. Rudd[*], Nathan R. Barton[*], Athanasios Arsenlis[*], Bruce A. Remington[*], Hye-Sook Park[*], Shon T. Prisbrey[*], Peter A. Vitello[*], Grant Bazan[*], Karnig O. Mikaelian[*], Andrew J. Comley[**], Brian R. Maddox[*] and Mark J. May[*]

[*]*Lawrence Livermore National Laboratory, Livermore, CA 94551*
[†]*Los Alamos National Laboratory, Los Alamos, NM 87545*
[**]*Atomic Weapons Establishment, Aldermaston, Reading RG7 4PR, United Kingdom*

Abstract. We present here the first dynamic Rayleigh-Taylor (RT) strength measurement of a material undergoing solid-solid phase transition. Iron is quasi-isentropically driven across the pressure-induced bcc (α-Fe) $\rightarrow$ hcp (ε-Fe) phase transition and the dynamic strength of the α, ε and reverted α' phases have been determined *via* proton radiography of the resulting Rayleigh-Taylor unstable interface between the iron target and high-explosive products. Simultaneous velocimetry measurements of the iron free surface yield the phase transition dynamics and, in conjunction with detailed hydrodynamic simulations, allow for determination of the strength of the distinct phases of iron. Forward analysis of the experiment *via* hydrodynamic simulations reveals significant strength enhancement of the dynamically-generated ε-Fe and reverted α'-Fe, compareable in magnitude to the strength of austenitic stainless steels.

Keywords: dynamic experiment, iron, phase transition, strength, proton radiography
PACS: 62.50-p, 62.20-x, 64.70-p, 64.70.K-

INTRODUCTION AND DESIGN SIMULATIONS

Iron is one of the most widely studied elemental materials in shock-wave physics, and the discovery of the reversible pressure-induced $\alpha \rightarrow \varepsilon$ (bcc$\rightarrow$hcp) phase transition goes back to the very origins of the field of shock compression of condensed matter.[1] While the equation of state of iron has been quite thoroughly studied, to date the dynamic strength of the high-pressure ε-Fe phase has been unknown. Here we report the first dynamic Rayleigh-Taylor strength measurement of both ε-Fe and the reverted α- phase (from here denoted α' to make the distinction that, while the underlying lattice is bcc there are significant microstructural differences from non-transitioned α-Fe). Knowledge of the high-pressure dynamic strength of ε-Fe may shed light on important questions in planetary science since the central region of the earth's core is believed to be ε-Fe.[2]

It can be shown that the presence of material strength stabilizes the solid phase against Rayleigh-Taylor instabilty (RTI).[3, 4, 5] The use of RTI as a measure of the dynamic strength of materials has been revisited in recent high pressure/high-strain rate laser experiments designed to access material states under extreme conditions.[6, 7] This experimental approach is also used here to study the dynamic strength of the high-pressure hcp phase of iron by using a high-explosive to quasi-isentropically ramp load an iron sample and radiograph the resulting Rayleigh-Taylor unstable interface.

Arbitrary Lagrangian/Eulerian (ALE) hydrodynamics calculations using a code developed at Lawrence Livermore National Laboratory (LLNL) were utilized for the preshot design of the experiments as well as the postshot analysis. Phase transitions of the material were simulated by enforcing a change in material equation of state (EOS) and strength state, on a zonal basis, when a critical pressure was achieved; once a zone has been phase transformed a reverse transition state may be applied when the resulting pressure falls below a critical value. This simulation methodology

has been shown capable of reproducing gas-gun experiments on iron[8, 9], including the complex 3-wave shock structure, with the exception of kinetic effects – the computational methodology described assumes infinitely fast kinetics. The focus of future computational efforts will be on exploring full stress-tensor dependence of the phase transition stress hysteresis[10], kinetics[11] and crystal scale models of the possible phase variants.[12]

The equations of state for α-Fe and ε-Fe used in the hydrocode simulations have been reported elsewhere[11] and shown to accurately represent the measured equilibrium phase fraction along the shock Hugoniot. The strain-rate dependent Preston-Tonks-Wallace (PTW) strength model[13] was used to represent the dynamic material strength of the distinct phases of iron, as its functional form reflects the physics of both the thermal activation (low strain-rate, accessible by classical strength experiments) and phonon drag (high strain-rate, informed by over-driven shock theory, molecular dynamics simulation, laser and pulsed power experiments) dislocation dynamics regimes.

Split-Hopkinson bar strength measurements of iron have been recently completed at LANL[14] over a range of temperatures (77-673 K) and strain-rate (0.001-4000 s^{-1}). Thermal activation regime PTW parameters for α-Fe were then fit to these stress-strain curves and used for (preshot) design calculations. Since the dynamic strength of ε-Fe was completely unknown prior to this study, the PTW parameters for α-Fe were also used for ε-Fe with the exception of the PTW parameter κ which was varied to reproduce the stress-strain response of reverted α'-Fe determined by post-shock recovery[15].

The previously described strength model was employed in all preshot design calculations; the results of these HE-driven Rayleigh-Taylor strength experiments described here have been used to further refine the dynamic strength in the phonon drag regime (*i.e.* the y_1, y_2, s_{drag} and β PTW parameters), and are given in Table 1. One additional feature to the PTW implementation used at LLNL is that the s_0 in the phonon drag term, $s_0(\dot{\psi}/\dot{\zeta})^{\beta}$, is distinct from the s_0 used in the thermal activation term (and denoted s_{drag}); having these equations uncoupled allows for greater flexibility in determining the work hardening while preserving stress-strain data in the thermal activation regime.

The LANL P-108 high-explosive plane wave lens, consisting of PBX 9501 and TNT, was simulated using the well-known JWL++ rate law and EOS.

The hydrodynamic simulations show that the quasi-shockless ramp compression results in a peak applied pressure of 280 kbar and peak strain-rate of 10^6 s^{-1} within the first μsec of the experiment, with pressures between 100-250 kbar and strain-rates on the order of 10^5 s^{-1} for the remaining ≈ 6 μsec.

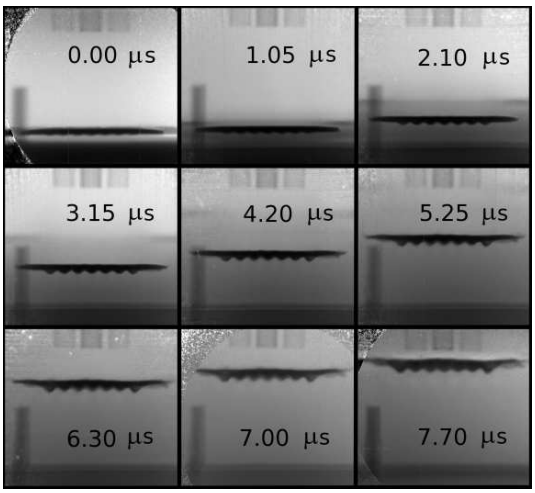

FIGURE 1. Proton radiographs of the dynamically loaded iron sample under study (note these frames are from a single experiment). Frames shown are representative of 7.7 μsec of the dynamic experiment after the high explosive products (applying a peak pressure of 280 kbar) have reached the sinusoidally perturbed interface. The initial amplitude of the sinusoidal perturbation is η_0=100 μm and after 7.7 μsec the perturbation has growth to 350 $\pm$ 35 μm due to the RTI. The suppression of RT growth is due to the dynamic material strength.

MATERIALS AND EXPERIMENTAL

The iron target was machined into a disc of diameter 31.75 mm. The initial sinusoidal perturbation was cut into the front surface (*i.e.* facing the explosive) by wire EDM, and consisted of a wavelength of λ=3 mm (with 7 nodes along the front face) and an amplitude of η_0=100 μm. Surface profilometry measurement verified that the amplitude was machined accurate to within 5 μm. A 5° bevel was machined along the back of the target (facing away from the HE) to minimize dynamic cupping of the sample due to the (relatively small) non-planarity of the HE plane wave lens.

Radiographs of the dynamic experiment were carried out using the 800 MeV proton radiography facility at the Los Alamos Neutron Science Center (LANSCE). The 3X proton magnifier was employed, yielding an effective 40 mm X 40 mm viewing area. The beam was focused by setting an energy loss of 20 MeV to correspond to the calculated ρr=9.0 g/cm^2 of the high-explosive products stagnating against the rippled side of the iron target.

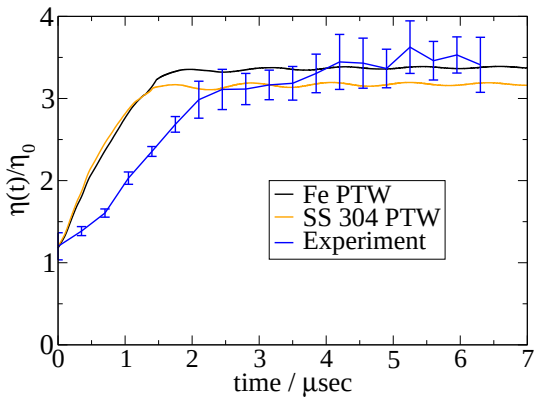

FIGURE 2. Rayleigh-Taylor growth of iron measured by proton radiography (blue) compared to hydrodynamic simulation utilizing a phase-aware Fe PTW strength model (black). To help illustrate the magnitude of the ε-Fe/α′-Fe strength, also shown is the iron material model with the PTW strength parameters of the austenitic stainless steel 304 applied to the ε and α′ phases.

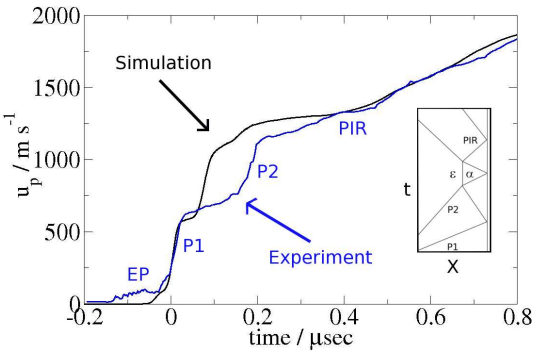

FIGURE 3. Photon doppler velocimetry, performed simultaneously with the proton radiography, clearly shows the onset of the phase transition. Following an elastic-plastic transition (EP), the α-Fe plastic wave (P1) is followed by the α-Fe→ ε-Fe phase transformation front (P2) moving through the material, with a phase interface reflection wave (PIR) present due to wave interaction with the standing α-Fe/ε-Fe interface (see inset). The 3-wave structure present in the velocimetry provides direct knowledge on the phase of the material observed in the proton radiography.

Each CCD camera of the imaging station 1 (6 cameras in total) provides 3 frames; each camera may be active no less than every 350 ns, with a 70 ns exposure time set in this experiment to maximize integrated proton flux while minimizing motion blur (based upon predicted target velocity). An additional 4 frames from imaging station 2 were interleaved along the dynamic trajectory to provide a total of 7.7 μsec of radiographic coverage, resulting in a high-quality 22 frame "movie" of the material under high-explosive drive. Features may be resolved down to approximately 40 μm, and it is possible to temporally space the cameras to extend the capture (and adjust exposure) as required for a particular experiment. The radiographic images were flat-fielded in intensity and the amplitude of RT interface was digitally extracted and quantified.

Photon doppler velocimetry (PDV) provided measurements of the particle velocity on the back of the iron target, and was performed simultaneously with the radiographic measurements. This measurement reveals the details of the stress wave moving through the material by providing the particle velocity, especially with regard to demonstrating the $\alpha \rightarrow \varepsilon$ phase transition, and also validates the time-dependent performance of the high-explosive (necessary for accurate hydrodynamic computer simulation of the resulting RTI).

RESULTS AND DISCUSSION

Representative series of proton radiographs of the perturbed iron surface under high-explosive drive for a duration of 7.7 μsec are shown in Figure 1; a total of 22 frames were acquired in the single experiment. The measured Rayleigh-Taylor growth factor, $\eta(t)/\eta_0$ along with the growth factor calculated *via* hydrodynamic simulation (utilizing the strength parameters given in Table 1) is reported in Figure 2. To put the magnitude of the high-pressure ε-Fe and reverted α′-Fe phases in context, the PTW strength model for the austenitic stainless steel 304 (from Reference [13]) was applied to the ε-Fe and α′-Fe materials in the hydrodynamic calculation. Conversely, simulation of the RT experiment utilizing only the α-Fe PTW parmeters for all phases of iron (not shown) exhibits a growth factor of ≈ 5, a 50 % enhancement to the RT growth factor over the simulations using the phase-aware model from Table 1. Given the aforementioned analysis, it is evident that ε-Fe/α′-Fe states exhibit significantly higher dynamic material strength than α-Fe, compareable in magnitude to stainless steel 304.

Simultaneous velocimetry of the target free surface is presented in Figure 3. The early time feature is the elastic precursor wave (EP), followed by the plastic wave (P1) created by α-Fe rushing in to meet phase transition front. The interaction of the phase transformation wave and the P1 reflection from the free surface lowered the stress in the phase transformation wave and results in a second plastic wave (P2). Interaction between the free-surface reflected P2 and the standing α/ε phase interface sends yet a third wave, the phase interface reflection (PIR), back toward the free surface. This coupling of stress

TABLE 1. PTW strength parameters found to reproduce the dynamic strength observed in the Fe RT experiments.

PTW Parameter	**α-Fe**	**ε-Fe/α′-Fe**
θ	0.015	0.015
p	3.0	3.0
s_0	0.01	0.01
s_∞	0.0025	0.0025
κ	0.35	0.30
γ	0.00001	0.00001
y_0	0.006625	0.006625
y_∞	0.00075	0.00075
y_1	0.006625	0.03
y_2	0.265	0.25
s_{drag}	0.01	0.03
β	0.265	0.25
α	0.23	0.23
G_0 / Mbar	0.872	0.872
T_m / K	1810	2050/1810

waves and phase transitions is a classic example in shock physics[8, 11] and we find the same phenomena under quasi-shockless loading here. More importantly for the present determination of strength, the velocimetry allows for the identification of the material phase under RT growth and also validates the high-explosive model in the hydrocode.

The PTW parameters for iron, found to best match both the high strain-rate (10^4-10^6 s^{-1}) Rayleigh-Taylor growth observed with proton radiography in the experiments here, and low strain-rate (10^{-3}-10^3 s^{-1}) split-Hopkinson bar experiments,[14] are reported in Table 1. α-Fe thermal activation parameters were determined from the split-Hopkinson bar data with the thermal activation paramters for ε-Fe/α′-Fe differing in κ from that of α-Fe to reproduce the stress-strain response of post-shock recovered α′-Fe experiments of Reference [15]. $\varepsilon - Fe/\alpha'$-Fe phonon drag parameters were determined by variation in the hydrocode to match the RT experiment reported here, while the α-Fe phonon drag term was calculated *via* overdriven shock theory.[16] The notion that the strength in the ε-Fe phase may vary greatly from that of α-Fe, and is thus described by a separate set of strength model parameters, is supported by the possibility that the dislocation kinetics in the new phase may be quite different even if dislocation density were essentially preserved.[17]. The ansatz that dislocation generation and/or twinning in the ε-Fe phase is then inherited by the reverted α′-phase[15] is assumed here by way of retaining identical strength parameters for both the ε and α′ phases. Future RT experiments on iron are planned that will elucidate the dynamic strength of ε-Fe and α′-Fe separately, and shed light on these important questions regarding phase transformations and plasticity.

ACKNOWLEDGMENTS

The authors give special thanks to the pRad team at LANSCE, especially Andy Saunders, Fesseha Mariam, Dale Tupa and Wendy McNeil for their expertise and dedication. JLB would like to thank Dana Rowley, Marina Bastea, Ted Perry and Brad Wallin (LLNL) for their insight and helpful discussions. This work was performed under the auspices of the U.S. DOE by LLNL under Contract DE-AC52-07NA27344.

REFERENCES

1. Bancroft, D., Peterson, E. L., and Minshall, S., *J. Appl. Phys.*, **27**, 291–298 (1956).
2. Tateno, S., Hirose, K., Ohishi, Y., and Tatsumi, Y., *Science*, **330**, 359–361 (2010).
3. Barnes, J. F., Blewett, P. J., McQueen, R. G., Meyer, K. A., and Venable, D., *J. Appl. Phys.*, **45**, 727–732 (1974).
4. Nadezhin, S., Ignatova, O., Igonin, V., Lebedev, A., Lebedeva, M., Podurets, A., Raevsky, V., Zocher, M., and Kaul, A., "Influence of dynamic properties on growth of perturbations in tantalum," in *Bulletin of the American Physical Society*, Nashville, TN, 2009.
5. Mikaelian, K. O., *Phys. Rev. E*, **54**, 3676–3680 (1996).
6. Park, H., Remington, B. A., Becker, R. C., Bernier, J. V., Cavallo, R. M., Lorenz, K. T., Pollaine, S. M., Prisbrey, S. T., Rudd, R. E., and Barton, N. R., *Phys. Plasmas*, **17**, 056314 (2010).
7. Park, H., Lorenz, K. T., Cavallo, R. M., Pollaine, S. M., Prisbrey, S. T., Rudd, R. E., Becker, R. C., Bernier, J. V., and Remington, B. A., *Phys. Rev. Lett.*, **104**, 135504 (2010).
8. Barker, L. M., and Hollenbach, R. E., *J. Appl. Phys.*, **45**, 4872–4877 (1974).
9. Jensen, B. J., Gray III, G., and Hixson, R. S., *J. Appl. Phys.*, **105**, 103502 (2009).
10. Lew, A., Caspersen, K., Carter, E. A., and Ortiz, M., *J. Mech. Phys. Solids*, **54**, 1276–1303 (2006).
11. Boettger, J. C., and Wallace, D. C., *Phys. Rev. B*, **55**, 2840–2849 (1997).
12. Barton, N. R., Benson, D. J., and Becker, R., *Modelling Simul. Mater. Sci. Eng.*, **13**, 707–731 (2005).
13. Preston, D. L., Tonks, D. L., and Wallace, D. C., *J. Appl. Phys.*, **93**, 211–221 (2003).
14. Gray III, G. T., Chen, S., and Olson, R. T., private communication.
15. Gray III, G. T., Hayes, D. B., and Hixson, R. S., *J. Phys. IV France*, **10**, Pr9755–Pr9760 (2000).
16. Chen, S., and Olson, R. T., private communication.
17. Barton, N. R., Arsenlis, A., Rhee, M., Marian, J., Bernier, J. V., Tang, M., and Yang, L., Submitted to the 2011 Proceedings of the American Physical Society Topical Meeting on the Shock Compression of Condensed Matter.